Nuclear Physics A556 (1993) 261–280
North-Holland

NUCLEAR
PHYSICS A

Coulomb excitation of ^{226}Ra

H.J. Wollersheim, H. Emling, H. Grein, R. Kulessa[1] and R.S. Simon
Gesellschaft für Schwerionenforschung, Darmstadt, Germany

C. Fleischmann, J. de Boer, E. Hauber, C. Lauterbach and C. Schandera
Sektion Physik, Ludwig-Maximilian-Universität, Munich, Germany

P.A. Butler
Oliver Lodge Laboratory, University of Liverpool, Liverpool, UK

T. Czosnyka
SLCJ, University of Warsaw, Warsaw, Poland

Received 30 May 1992
(Revised 14 September 1992)

Abstract: Radioactive targets of ^{226}Ra were Coulomb excited by ^{4}He projectiles (particle spectroscopy), and ^{16}O, ^{32}S and ^{208}Pb projectiles (particle-γ coincidences). The $K = 0^{\pm}$ rotational bands could be followed up to spin 18^{+} and 17^{-}, respectively. All experiments were simultaneously analyzed in terms of E1, E2, E3 and E4 matrix elements coupling the positive- and negative-parity rotational states. The systematics of level energies, as well as dipole, quadrupole and octupole matrix elements are discussed in the framework of models assuming stable octupole deformation.

E | NUCLEAR REACTIONS ^{226}Ra(^{4}He, ^{4}He'), $E = 15$–17 MeV; ^{226}Ra(^{16}O, ^{16}O'), $E = 63$ MeV; ^{226}Ra(^{32}S, ^{32}S'), $E = 135$ MeV; ^{226}Ra(^{208}Pb, ^{208}Pb'), $E = 978$ MeV; measured $\sigma(E_\gamma, \vartheta_\gamma, \Theta_\rho)$, pp$\gamma(\Theta)$-coin. ^{226}Ra deduced levels, I, B(E1), B(E2), B(E3), B(E4), quadrupole moment. Enriched targets.

1. Introduction

Evidence has increased during the last few years that certain nuclei can be described in terms of intrinsic shapes with parity-breaking static moments. In particular, the discovery [1]) of very low-lying 1^{-} states in the light actinides has led to the suggestion of stable octupole deformations. It has been recognized [2]) that the microscopic origin for the occurrence of this structure lies in the coupling between single-particle states which differ by $\Delta l = 3$ and $\Delta j = 3$. These states lie close to each other and to the Fermi surface at proton and neutron numbers near 34, 56, 88 and 134 where octupole correlations are expected to be strongest. Fig. 1 (top) shows

Correspondence to: Dr. H.J. Wollersheim, GSI, Postfach 110 552, D-6100 Darmstadt 11, Germany.
[1] Permanent address: Jagellonian University, Cracow, Poland.

0375-9474/93/$06.00 © 1993 – Elsevier Science Publishers B.V. All rights reserved

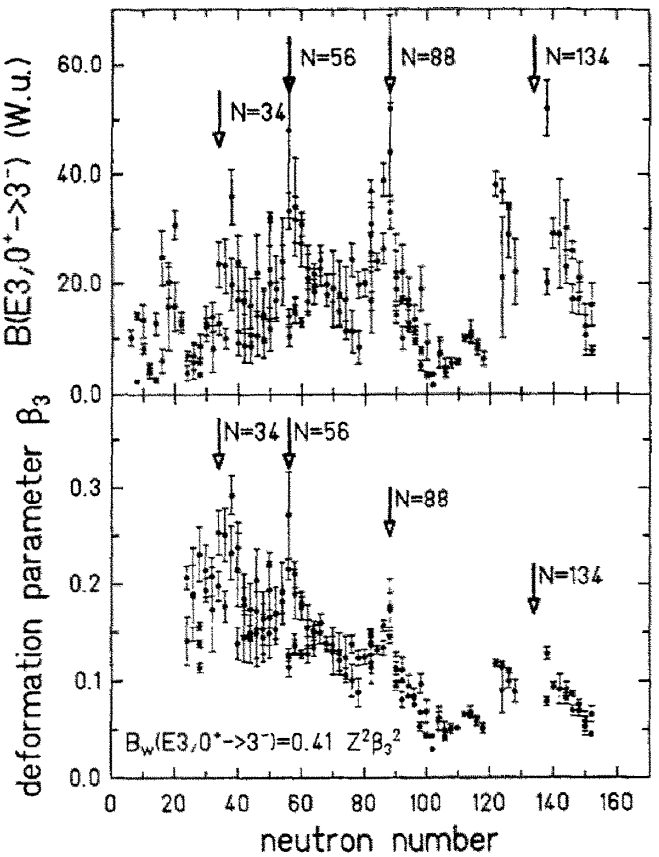

Fig. 1. Reduced transition rate $B(\mathrm{E3};\ 0^+ \rightarrow 3^-)$ in W.u. (top) and of the octupole deformation parameter β_3 (bottom) as a function of neutron number.

the systematics of experimental $B(\mathrm{E3};\ 0^+ \rightarrow 3^-)$ values for even-A nuclei [3]) as a function of neutron number. It shows enhanced octupole collectivity at the expected particle numbers. These $B(\mathrm{E3})$ values, given in Weisskopf units (W.u.), can be related to a deformation parameter β_3 (see fig. 1 bottom) using the expression.

$$B(\mathrm{E3};\ 0^+ \rightarrow 3^-) = 0.409 Z^2 \beta_3^2 \quad \text{(W.u.)} \tag{1}$$

if one assumes a stable octupole deformation in the intrinsic frame. This procedure is model dependent and assumes a uniform charge distribution with a sharp cut-off radius. For nuclei with collective $B(\mathrm{E3})$ values the extracted β_3 deformation parameters are of similar value as the quadrupole deformation. In addition to this systematics observed at low spins, further evidence for the presence of strong octupole correlations can be found from the high-spin properties of nuclei. The energy spectra of octupole-deformed nuclei resemble those of asymmetric diatomic

molecules. The observed positive- and negative-parity states for even-A nuclei are regarded as a single rotational band of an octupole-deformed core. They are connected by enhanced E1 transitions which are interpreted as manifestation of an intrinsic dipole moment. This moment is expected to arise from the polarization of the nucleus, induced by a separation of the centre-of-charge from the centre-of-mass in the intrinsic frame due to octupole correlations.

Experimentally, the limited number of suitable beam-target combinations makes it difficult to investigate octupole correlation effects in light actinide nuclei systematically. Data from (HI, xn) reactions are presently restricted to Ra and Th isotopes with $A \leq 220$ and $A \leq 224$, respectively. An extension to the heavier isotopes is difficult with present techniques due to the overwhelming competition of fission following the formation of the compound nucleus to be studied. The availability of targets of the quasi-stable nucleus ^{226}Ra ($T_{1/2} = 1600$ y) has, however, opened the possibility to investigate by Coulomb excitation this nucleus which is not accessible by (HI, xn) reactions.

The details of the experiment are described in sect. 2. In sect. 3, the level scheme of ^{226}Ra is presented. From the experimental cross sections, the collective properties of these levels have been deduced. The analysis of the electromagnetic matrix elements is also described in this section. A discussion of the experimental findings and the summary are presented in sects. 4 and 5, respectively.

2. Experimental procedures

The present Coulomb-excitation experiments on ^{226}Ra were performed using the ^{4}He, ^{16}O and ^{32}S beam from the Munich tandem accelerator and the ^{208}Pb beam from the UNILAC at GSI laboratory in Darmstadt. The data were taken at beam energies low enough to ensure negligible interference from nuclear forces.

2.1. INELASTIC SCATTERING OF ^{4}He

The ^{4}He experiment was performed at energies between 15 and 17 MeV and at scattering angles of 120° and 145°. The elastically and inelastically scattered ^{4}He particles were detected in the focal plane of a Q3D spectrograph by a 100-cm-long position-sensitive proportional counter. Isotopically pure targets were prepared by evaporating 12 μg/cm^2 and 60 μg/cm^2 ^{226}RaBr$_2$ on 50 μg/cm^2 C-backings. A spectrum of 16 MeV ^{4}He particles, scattered from ^{226}Ra is shown in fig. 2. The peaks corresponding to scattering from 0^+, 2^+, 4^+ and 3^- states can clearly be distinguished. The measured excitation probabilities of the 2^+ and 3^- states provide information on the E2 and E3 matrix elements connecting them to the ground state. A comparison of the 4^+ excitation by ^{4}He with that by ^{16}O ions allows the contribution from the E2–E2 cascade to be separated from the E4 contribution.

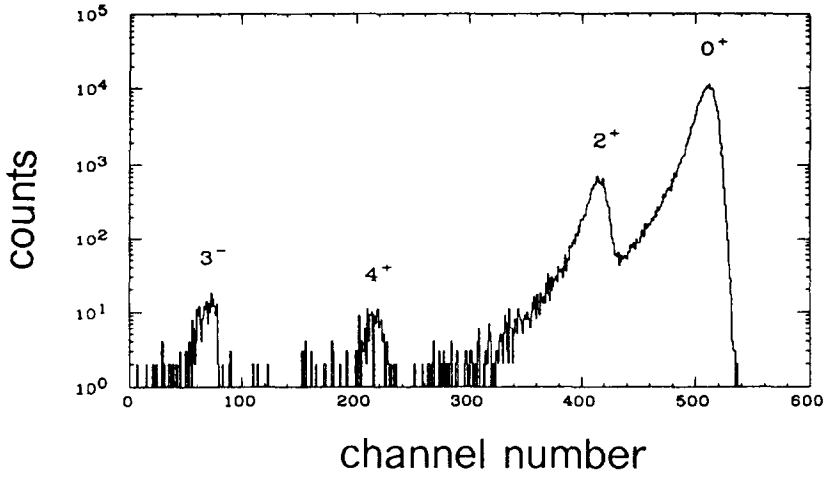

Fig. 2. Energy spectrum of 16 MeV α-particles scattered from ^{226}Ra at a laboratory angle of 145°

2.2. GAMMA-PARTICLE COINCIDENCES WITH ^{16}O AND ^{32}S PROJECTILES

The Munich tandem accelerator was used to produce projectiles of 63 MeV ^{16}O and of 135 MeV ^{32}S. The target consisted of 3 mm diameter spots of $^{226}RaBr_2$ with a thickness of 170 $\mu g/cm^2$ evaporated onto 50 $\mu g/cm^2$ carbon and covered by a layer of 40 $\mu g/cm^2$ beryllium. The particle detector was a position-sensitive annular parallel-plate avalanche-counter subtending a range from $\vartheta_{lab} = 112°$ to $\vartheta_{lab} = 168°$ with a resolution better than 9° in the scattering angle ϑ and a resolution of 18° in the azimuthal angle φ. The energy loss of the backscattered ^{32}S projectiles is sufficiently larger than that of the α-articles from the radioactive target to separate the two groups. The coincidence spectrum was contaminated by background from the source activity, which could not be fully separated from the ^{16}O signals. The γ-detectors were four lithium-drifted germanium diodes placed in a plane at 0°, ±70° and 180° (annular Ge(Li) counter) with respect to the beam direction, at a distance of 11 to 12 cm. The γ-spectra were corrected for Doppler shift before analyzing the line intensities.

2.3. GAMMA-PARTICLE COINCIDENCES WITH ^{208}Pb PROJECTILES

The UNILAC at GSI laboratory provided 4.7 MeV/u ^{208}Pb projectiles impinging on a 400 $\mu g/cm^2$ ^{226}Ra target sandwiched between 40 $\mu g/cm^2$ Be and 50 $\mu g/cm^2$ C.

The experimental setup used for the measurement of particle-γ coincidence spectra is shown in fig. 3. Both the recoiling target nuclei and the scattered projectiles were detected in an arrangement of five positon-sensitive parallel-plate avalanche gas-counters: an annular detector ($15° \leq \vartheta_{lab} \leq 45°$, $0° \leq \varphi_{lab} \leq 360°$) and four rectangular particle detectors symmetrically placed around the beam axis, each covering an

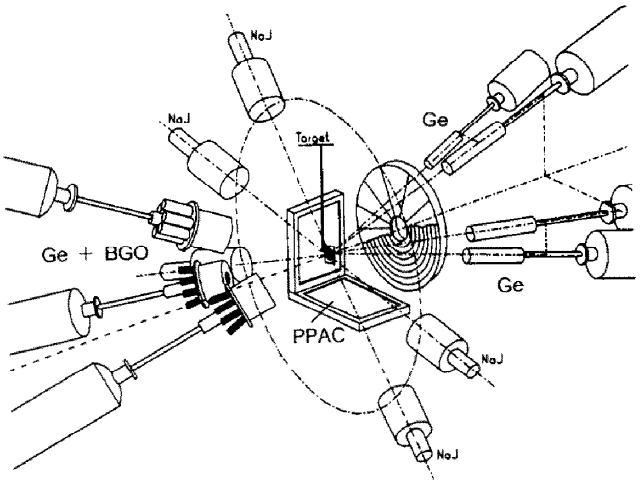

Fig. 3. Experimental set-up used in Coulomb excitation experiments with ^{208}Pb beams. Ge and BGO denote the Ge detectors and the Compton suppression shields, respectively. For the detection of projectiles and target nuclei, parallel-plate avalanche gas counters (PPAC) were used.

angular range of $53° \leq \vartheta_{lab} \leq 90°$ and $0° \leq \varphi_{lab} \leq 84°$. The particle detectors were made position sensitive in the scattering-angle direction (ϑ_{lab}) by means of a special delay-line readout incorporated into the multi-strip detector-anode. The information about the azimuth angle (φ_{lab}) was obtained by dividing the thin metalized cathode foil of the annular detector into 20 radial segments of 18° each. By measuring the kinematical correlation between the scattering angles of both reaction partners, the recoiling ^{226}Ra nucleus could be identified uniquely. The coincident emission of γ-rays was observed in seven Ge detectors (three of them Compton suppressed) positioned at angles of 30° and 150° with respect to the beam direction. In addition a multiplicity filter of six NaI detectors was installed at 90° to enable selection of events of high γ-multiplicity. The information about the scattering angle of the excited Ra nucleus allowed corrections to be made for the large Doppler shifts of the emitted γ-rays due to the high recoil velocities (up to $\sim 10\%\ c$). Moreover, the measurement of the scattering angles provided the impact-parameter dependence of the Coulomb excitation process, allowing to determine individual E1, E2 and E3 matrix elements.

The summed γ-ray spectrum of all Ge detectors, after Doppler-shift correction and suppression of the Compton background, obtained for the ^{226}Ra + ^{208}Pb system at a bombarding energy of 4.7 MeV/u is displayed in fig. 4. To generate this spectrum it was required that one of the collision partners was detected in the angular range of $15° \leq \vartheta_{lab} \leq 45°$ and at least one γ-ray was detected by the NaI array. Transitions up to $18^+ \rightarrow 16^+$ and $17^- \rightarrow 15^-$ can be assigned in the ground-state ($K = 0^+$) and in the low-lying negative-parity band ($K = 0^-$), respectively. The energy resolution was about 3 keV for the high-spin transitions in the Pb experiment.

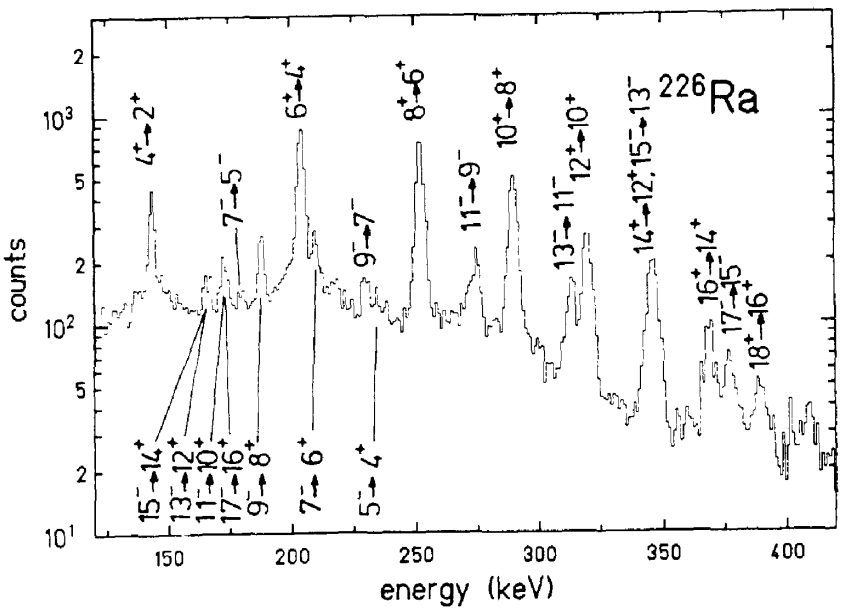

Fig. 4. Doppler-shift corrected spectrum of γ-rays following the Coulomb excitation of ^{226}Ra by a 4.7 MeV/u ^{208}Pb beam.

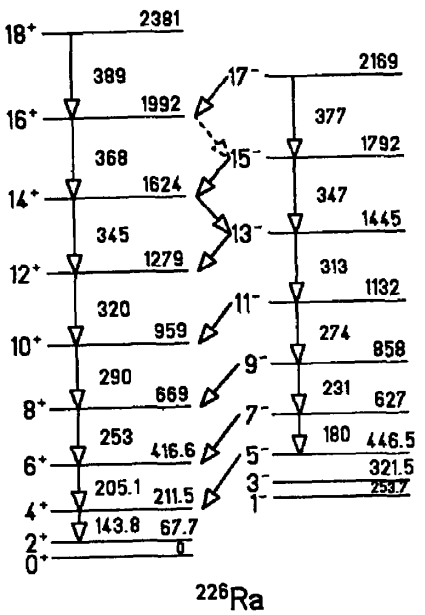

Fig. 5. Partial level scheme of ^{226}Ra and the transitions observed in the present experiment.

3. Experimental results

3.1. PARTIAL LEVEL SCHEME OF ^{226}Ra

A partial level scheme of ^{226}Ra showing the γ-transitions observed in our experiments is presented in fig. 5 and confirms the low-spin data of an earlier work [28]). The spin assignments were obtained from the systematic impact-parameter dependence of the γ-ray yields, from the particle-γ directional correlation, and from γ-multiplicity measurements. For the lower spin states the $\gamma\gamma$-coincidence matrix accumulated from the data of ^{16}O and ^{32}S experiments verifies the cascade relationship up to the $10^+ \rightarrow 8^+$ and $9^- \rightarrow 8^+$ transitions, respectively. The $K = 0^+$ bands could be followed up to spin $I^\pi = 18^+$ and $I^\pi = 17^-$, respectively. Down to spin $I \sim 7\hbar$, the level structure of ^{226}Ra shows the interleaving even-odd spin sequence characteristic for nuclei with stable octupole deformation. At low excitation energy the even-odd spin sequence is not developed and the level scheme exhibits the signature of an octupole-vibrational nucleus.

The observation of the even-odd spin sequence at moderately high spins has been interpreted as evidence that the octupole deformation stabilizes with increasing rotational frequency. Nazarewicz and Olanders [4]) have introduced the energy displacement δE of the negative-parity states with respect to the position expected from the energies of the neighbouring positive-parity states assuming that both, negative and positive-parity states, form a regular rotational band:

$$\delta E = E(I)^- - \frac{IE(I+1)^+ + (I+1)E(I-1)^+}{2I+1}. \tag{2}$$

Fig. 6 shows δE versus spin I for $^{218-226}$Ra. The energy displacement varies from large positive values at lower spins to relatively small negative values at high spin ($\delta E = 0$ would correspond to the ideal octupole - deformation case). The pattern of the ^{226}Ra levels is seen to follow the stable octupole limit rather closely above $I = 11\hbar$.

Another nuclear property sensitive to strong octupole correlations is the moment of inertia of a deformed nucleus. The high-j intruder states, such as the proton $i_{13/2}$ and the neutron $j_{15/2}$ states in the actinide region, are strongly aligned by the rotation and therefore they are the main contributors to the high angular-momentum in rotating nuclei. As a result of the quasi-particle alignment the moment of inertia exhibits a backbending behaviour as a function of the rotational frequency ω. Cranked Hartree-Fock-Bogolyubov [5]) as well as cranked shell-model calculations [6]), using single-particle potentials with only even-parity deformation modes, were performed for nuclei in the vicinity of ^{226}Ra. They predict backbending at spins around $I = 18\hbar$ and at $\hbar\omega \leqslant 0.20$ MeV in ^{226}Ra whereas calculations admitting an octupole deformation of the potential do not predict backbending [4]). This is because the octupole interaction mixes the high-spin intruder states with the close-lying low angular-momentum orbitals of the opposite parity. The aligned angular

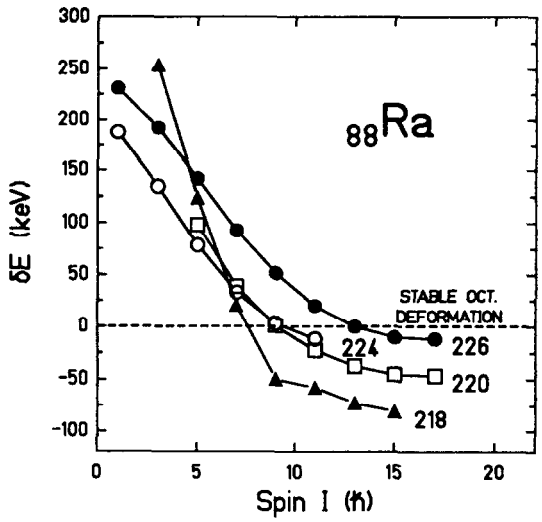

Fig. 6. Displacement energy δE of the positive- and negative-parity bands in the Ra isotopes.

moment is therefore reduced substantially and a smooth upbending is predicted rather than a backbending.

This is exactly what has been observed for ^{226}Ra: In fig. 7 the aligned angular momentum i in the ground-sate band and in the negative-parity band of ^{226}Ra is plotted as a function of the rotational frequency $\hbar\omega$. The quantity i is calculated from the experimental spins and level energies following the prescription of ref. [7]). The alignment in the ground-state band sets in at $\hbar\omega \sim 0.15$ MeV and shows a gradual increase up to the highest frequencies observed. In the negative-parity band the alignment seems to saturate slightly below $2\hbar$. Experimentally, there is no sign

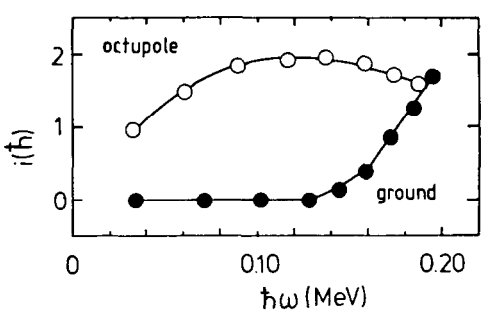

Fig. 7. Aligned angular momentum i in the ground-state band and in the negative-parity (octupole) band of ^{226}Ra. The spin i is obtained by subtracting the collective spin

$$I_{\text{coll}} = 43.3\omega\ (\hbar^2/\text{MeV}) + 1006\omega^3\ (\hbar^4/\text{MeV}^3)$$

from the classical estimate $I + \frac{1}{2}$ (with ω being the rotational frequency).

of backbending in ^{226}Ra. This gives further support of the octupole deformation picture.

3.2. ANALYSIS OF COULOMB-EXCITATION CROSS SECTIONS

The population of a nuclear state by multiple Coulomb excitation and its subsequent decay depends on various electromagnetic matrix elements. At low transition energies, the process of internal conversion plays an important role. The matrix elements determine the excitation paths as well as the feeding from higher levels. The excitation process is mainly determined by E2 and E3 matrix elements, whereas the decay may contain M1 and E1 transitions. A unique determination of the matrix elements can only be achieved if the impact-parameter dependence of the γ-ray yields is measured over a wide range of scattering angles for heavy projectiles. In the present study the inelastic cross sections were therefore measured for ^{4}He, ^{16}O, ^{32}S and ^{208}Pb projectiles at bombarding energies well below the Coulomb barrier.

3.2.1. Matrix elements from inelastic-scattering cross sections. In the ^{4}He-scattering experiment, the excitation cross sections for the 2^+, 4^+ and 3^- state were determined relative to the elastic (0^+) intensity. The reduced transition probabilities between the ground state and the various excited states were obtained by comparing the measured excitation cross sections with those calculated by a semiclassical coupled-channel code [8,9]). All quadrupole (E2), octupole (E3) and hexadecapole (E4) matrix elements connecting the 0^+, 2^+, 3^- and 4^+ states were included in these calculations. The matrix elements connnecting the states can be converted to reduced transition probabilities, $B(\mathrm{E}\lambda; 0\rightarrow\lambda)$. The values obtained from the present study are listed in table 1.

For a rigid rotor the measured transition probabilities are related to the intrinsic multipole moments by

$$B(\mathrm{E}\lambda, 0\rightarrow\lambda) = \frac{(2\lambda+1)}{16\pi} e^2 Q_\lambda^2 . \tag{3}$$

For a homogeneous charge distribution of shape $R = R_0(1+\beta_2 Y_{20}+\beta_3 Y_{30}+\beta_4 Y_{40})$, the deformation parameters β_2, β_3 and β_4 can be calculated from the intrinsic

TABLE 1

Reduced transition probabilities and charge deformation parameters in ^{226}Ra

λ	$B(\mathrm{E}\lambda; 0\rightarrow\lambda)[e^2\mathrm{b}^\lambda]$	β_λ (exp)	β_λ [ref. [10]]
2	5.15(14)	+0.165(2) [a]	+0.164
3	1.10(11)	0.104(5)	−0.112
4	1.08(15)	0.123(8)	+0.096

[a]) Sign of deformation parameter was determined from the static E2 moment.

multipole moments using the following implicit expressions:

$$Q_2 = \frac{3ZR_0^2}{\sqrt{5\pi}}(\beta_2 + 0.360\beta_2^2 + 0.336\beta_3^2 + 0.328\beta_4^2 + 0.967\beta_2\beta_4 + \cdots), \quad (4a)$$

$$Q_3 = \frac{3ZR_0^3}{\sqrt{7\pi}}(\beta_3 + 0.841\beta_2\beta_3 + 0.769\beta_3\beta_4 + \cdots), \quad (4b)$$

$$Q_4 = \frac{ZR_0^4}{\sqrt{\pi}}(\beta_4 + 0.725\beta_2^2 + 0.462\beta_3^2 + 0.411\beta_4^2 + 0.983\beta_2\beta_4 + \cdots). \quad (4c)$$

For a charge radius parameter $R_0 = 1.2A^{1/3}$ fm, we have evaluated the above relationships numerically to extract the values for β_2, β_3 and β_4 given in table 1. The resulting quadrupole (β_2), octupole (β_3) and hexadecapole (β_4) deformation parameters are in excellent agreement with theoretical values [10]) for a stable octupole deformation of ^{226}Ra.

3.2.2. Matrix elements from gamma-ray yields after Coulomb excitation. For the heavier projectiles the Coulomb-excitation cross sections are obtained from the observed de-excitation γ-ray yields. E1, E2 and E3 reduced matrix elements were extracted from experimental gamma yields using the semiclassical Coulomb-excitation least-squares search code GOSIA [11]). A total of 475 efficiency-corrected experimental gamma intensities from 20 data sets corresponding to different projectiles and different scattering angles were all fitted in one single analysis. Calculated gamma intensities were corrected for internal conversion, as well as the attenuation of the particle-γ angular correlation due to deorientation of the nuclei recoiling into vacuum and for the finite size of the Ge detectors. Relativistic distortion of the angular distributions due to the motion of the decaying recoil nuclei was also taken into account. Details of the analysis can be found in ref. [12]).

When analysing the ^{226}Ra Coulomb excitation data one has to consider the relative sign of the E1, E2 and E3 matrix elements. If the signs of all E1 and E3 intrinsic moments are changed with respect to the E2 moments, the excitation amplitudes of the octupole band will have a different sign, but the excitation probabilities remain the same. This is because only the odd-order products of E1 and E3 matrix elements are involved in the excitation of this band while only even-order products of these matrix elements are responsible for the excitation of the positive-parity states. The choice of the opposite sign of the E1 intrinsic moment with respect to the E3 intrinsic moment will, however, change the interference term and hence the excitation probabilities. The overall effect is found to be rather small, since E1 excitation is almost negligible as compared to the E2 and E3 excitations. Nevertheless, both sign combinations were independently evaluated. The resulting χ^2 values are nearly the same (0.83 for negative E1 * E3 product, 0.84 for positive E1 * E3 product), indicating that the data used in this analysis are not sufficiently accurate to determine the relative sign of the E1 and E3 matrix elements. The difference

between the magnitude of the matrix elements corresponding to both minima is for all of them much smaller than the error bars ascribed to both solutions; therefore we took the average of the two magnitudes and assigned errors covering both combinations of signs as a final experimental result (tables 2–4).

In our analysis 131 E1, E2, E3 and E4 matrix elements were used to describe the coupling scheme. Out of this number about 60 were significant, i.e. their influence on the observed γ-intensities was sufficient to determine them with reasonable accuracy. The uniqueness of the solution was tested using different sets of starting values for minimization to check whether it converges to the same final set of matrix elements.

The matrix elements – parameters of the minimization – are strongly correlated. This correlation has to be taken into account when the errors of the fitted matrix elements are evaluated. The error estimation procedure of GOSIA, described in detail in ref. [11]), first establishes a "maximum correlation direction" in the space of matrix elements for each matrix element individually. This direction is defined as a vector along which the increase of χ^2 is the least when moving away from the minimum. Then, for each matrix element, the standard confidence limits are found along the axis. Using this approach one does not need to assume locally quadratic behaviour of χ^2 around the minimum. The procedure outlined above is especially suited to the situation in which the true minimum is not perfectly reached.

One of the possible sources of systematic errors is neglecting the matrix elements of higher multipolarities. In the present study E1, E2, E3 and E4 matrix elements were included. In contrast to results for light ions, heavy-ion data are almost

TABLE 2

Experimental E1 matrix elements for transitions in ^{226}Ra

$I_i \to I_f$	$\langle I_f \| M(\mathrm{E1}) \| I_i \rangle$ ($e \cdot$ fm)
$0^+ \to 1^-$	0.050 ± 0.009
$1^- \to 2^+$	0.068 ± 0.010
$2^+ \to 3^-$	0.061 ± 0.007
$3^- \to 4^+$	0.057 ± 0.005
$4^+ \to 5^-$	0.093 ± 0.007
$5^- \to 6^+$	—
$6^+ \to 7^-$	0.157 ± 0.010
$7^- \to 8^+$	0.21 ± 0.08
$8^+ \to 9^-$	0.24 ± 0.02
$9^- \to 10^+$	0.27 ± 0.05
$10^+ \to 11^-$	0.33 ± 0.04
$11^- \to 12^+$	0.35 ± 0.08
$12^+ \to 13^-$	0.63 ± 0.08
$13^- \to 14^+$	$0.65^{+0.15}_{-0.05}$
$14^+ \to 15^-$	—
$15^- \to 16^+$	$0.55^{+0.07}_{-0.14}$

TABLE 3

Experimental E2 matrix elements for transitions in ^{226}Ra

$I_i \rightarrow I_f$	$\langle I_f \|\| M(\mathrm{E2}) \|\| I_i \rangle$ ($e \cdot \mathrm{fm}^2$)
$0^+ \rightarrow 2^+$	$+226 \pm 1$
$2^+ \rightarrow 4^+$	$+370^{+9}_{-5}$
$4^+ \rightarrow 6^+$	$+483^{+6}_{-7}$
$6^+ \rightarrow 8^+$	$+541^{+7}_{-10}$
$8^+ \rightarrow 10^+$	$+591^{+24}_{-11}$
$10^+ \rightarrow 12^+$	$+900^{+21}_{-37}$
$12^+ \rightarrow 14^+$	$+732^{+51}_{-22}$
$14^+ \rightarrow 16^+$	$+821^{+190}_{-62}$
$16^+ \rightarrow 18^+$	$+559^{+75}_{-59}$
$2^+ \rightarrow 2^+$	-147^{+32}_{-29}
$4^+ \rightarrow 4^+$	-338^{+47}_{-32}
$6^+ \rightarrow 6^+$	-577^{+37}_{-75}
$8^+ \rightarrow 8^+$	-565^{+136}_{-27}
$10^+ \rightarrow 10^+$	-487^{+144}_{-50}
$12^+ \rightarrow 12^+$	-515^{+150}_{-180}
$1^- \rightarrow 3^-$	$+366^{+6}_{-12}$
$3^- \rightarrow 5^-$	$+409^{+5}_{-10}$
$5^- \rightarrow 7^-$	$+407^{+3}_{-7}$
$7^- \rightarrow 9^-$	$+545^{+3}_{-17}$
$9^- \rightarrow 11^-$	$+677^{+30}_{-70}$
$11^- \rightarrow 13^-$	$+1000^{+110}_{-70}$
$13^- \rightarrow 15^-$	$+970^{+300}_{-220}$
$1^- \rightarrow 1^-$	-415^{+25}_{-35}
$3^- \rightarrow 3^-$	-452^{+110}_{-60}
$5^- \rightarrow 5^-$	-482^{+61}_{-44}
$7^- \rightarrow 7^-$	-595^{+71}_{-148}
$9^- \rightarrow 9^-$	-677^{+145}_{-114}

insensitive to E4 couplings, as predicted by GOSIA simulations. Nevertheless, a test to estimate the influence of E4 matrix elements on the fitted E1, E2 and E3 values was conducted. The magnitude of E4 matrix elements included in the coupling scheme were increased by 50% and the fitting redone, keeping the E4 matrix elements fixed. Comparison of the best solution and the resulting minimum showed no discrepancies exceeding the quoted errors. For example, the values of $\langle 1 \| M(\mathrm{E1}) \| 0 \rangle$, $\langle 2 \| M(\mathrm{E2}) \| 0 \rangle$ and $\langle 3 \| M(\mathrm{E3}) \| 0 \rangle$ matrix elements changed by 2%, 0.5% and 2.5%, respectively. A similar test was done to check the influence of virtual excitation of giant dipole resonance (GDR). This effect is taken into account following the prescription of ref. [8]). The fit with GDR correction switched off yielded 10%, 0.5% and 1% change for the matrix elements listed above. Finally, the effect of unobserved side bands has been simulated by including a 2^+ state at 1.1 MeV (energy region where some levels are known to exist) coupled to the observed levels with the matrix

TABLE 4

Experimental E3 matrix elements for transitions in ^{226}Ra. The phase of the negative-parity wave functions was chosen by assuming $\langle 3||M(\mathrm{E3})||0\rangle$ to be positive

$I_i \rightarrow I_f$	$\langle I_f\|\|M(\mathrm{E3})\|\|I_i\rangle$ $(e\cdot \mathrm{fm}^3)$
$0^+ \rightarrow 3^-$	$+1080 \pm 30$
$2^+ \rightarrow 1^-$	$+1190^{+30}_{-70}$
$2^+ \rightarrow 3^-$	-1150 ± 160
$2^+ \rightarrow 5^-$	$+2000 \pm 70$
$4^+ \rightarrow 1^-$	-1470^{+160}_{-70}
$4^+ \rightarrow 3^-$	$+1450^{+320}_{-140}$
$4^+ \rightarrow 5^-$	> -1700
$4^+ \rightarrow 7^-$	$+2450^{+70}_{-140}$
$6^+ \rightarrow 3^-$	-2600 ± 500
$6^+ \rightarrow 5^-$	$+2000 \pm 300$
$6^+ \rightarrow 7^-$	-2400^{+1400}_{-400}
$6^+ \rightarrow 9^-$	$+2900^{+100}_{-200}$
$8^+ \rightarrow 5^-$	> -2400
$8^+ \rightarrow 11^-$	$+2200^{+600}_{-1700}$

elements chosen in such a way that resulting γ-yields are above the limit of observability. The fitting procedure yielded the changes in the lowest E1, E2 and E3 matrix elements of 6%, 1.5% and 6%, respectively. All these estimates are to be considered as upper limits. In addition the effect of E5 matrix elements (assuming $\beta_5 = 0.5 \times \beta_3$ and rigid-rotor spin dependence) was found to be insignificant. The E4 matrix elements were included in the fit as well as GDR correction.

4. Discussion of the electromagnetic moments

4.1. COLLECTIVE QUADRUPOLE AND OCTUPOLE MOMENTS

The predominantly collective character of the Coulomb excited states of ^{226}Ra is reflected by the large E2 and E3 matrix elements obtained in the present experiment. The corresponding reduced transition probabilities $B(\mathrm{E}\lambda)$ have values up to 126 and 52 single-particle units, respectively. Consequently, the following discussion of the observed electromagnetic moments will be concentrated on collective parameters, especially the quadrupole and octupole deformation.

The quadrupole shape of a nucleus is usually described by the β_2 and γ deformation parameters. The parameter β_2 can be determined from the reduced transition probability $B(\mathrm{E2}; 0 \rightarrow 2)$. It is interesting to note that this value is only slightly changed when axial symmetry of the nucleus is violated (maximum deviation 7% for $\gamma = 20°$). The most direct data on the γ degree of freedom can be obtained by measuring the spectroscopic quadrupole moments $Q_s(I)$ in the excited states. The

ensemble of our experimental results yields a nearly complete set of matrix elements of the quadrupole operator for collective states of the yrast band. For reasons becoming obvious below, we transform the measured diagonal matrix elements $\langle I||M(\mathrm{E2})||I\rangle$ in the ground-state band according to the expression

$$\frac{Q_s(I)}{Q_2}=\sqrt{\frac{I(2I-1)}{(I+1)(2I+1)(2I+3)}}\,\frac{\langle I||M(\mathrm{E2})||I\rangle}{\langle 2||M(\mathrm{E2})||0\rangle}, \tag{5}$$

where Q_2 is the intrinsic quadrupole moment of an axially symmetric nucleus. The values of the spectroscopic quadrupole moment (in units of Q_2) in the ground band of ^{226}Ra are shown in the upper part of fig. 8 and are compared with predictions of the rigid asymmetric rotor model [13]). As seen in fig. 8 there is a straightforward procedure to deduce the quadrupole shape parameter γ from the spectroscopic quadrupole moments $Q_s(I)$ in the ground-state band. The data favour a γ-value around 0°. However, the observed deviations may indicate a softness of the nuclear shape as discussed in the extended asymmetric rotor model [29]).

Since the γ-deformation seems to be small, the reduced matrix elements are expressed in terms of intrinsic moments Q_λ, using the axially symmetric rigid-rotor expressions:

$$\langle I-1||M(\mathrm{E1})||I\rangle=\sqrt{\frac{3}{4\pi}}\sqrt{I}\,eQ_1\,, \tag{6a}$$

$$\langle I-2||M(\mathrm{E2})||I\rangle=\sqrt{\frac{15}{32\pi}}\sqrt{\frac{I(I-1)}{2I-1}}\,eQ_2\,, \tag{6b}$$

$$\langle I-3||M(\mathrm{E3})||I\rangle=\sqrt{\frac{35}{32\pi}}\sqrt{\frac{(I-2)(I-1)I}{(2I-3)(2I-1)}}\,eQ_3\,. \tag{6c}$$

The measured $\langle I_f||M(\mathrm{E}\lambda)||I_i\rangle$ matrix elements (tables 2–4) are related to the reduced transition probabilities $B(\mathrm{E}\lambda)$ by

$$B(\mathrm{E}\lambda, I_i\to I_f)=\frac{1}{2I_i+1}\langle I_f||M(\mathrm{E}\lambda)||I_i\rangle^2\,. \tag{7}$$

From our measurements we are able to determine most of the electric dipole Q_1, quadrupole Q_2 and, for the first time, octupole Q_3 transition moments up to spin 18 for the yrast states. The experimental data on the intrinsic electric multipole moments are summarized in figs. 8 and 9. The quadrupole moments of both, positive- and negative-parity states, are very similar ($Q_2\approx 750\,\mathrm{fm}^2$) as expected for levels forming a single rotational band. A significant spin dependence of the transition quadrupole moments is not observed (see fig. 8).

The octupole deformation is determined by the E3 transition moments which are less sensitive to single-particle effects than the intrinsic dipole moments. The average

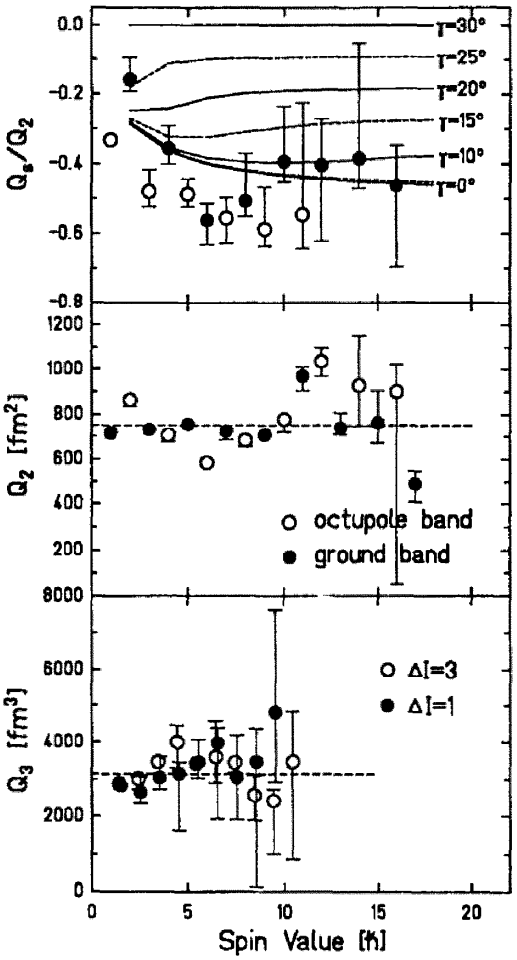

Fig. 8. Ratio of the quadrupole moments Q_s/Q_2 (top), electric transition quadrupole moments Q_2 (center) and octupole moments Q_3 (bottom) for the yrast band in ^{226}Ra.

Q_3 values at high spins are well described by a rigid rotor with an intrinsic moment $Q_3 = 3100\,\mathrm{fm}^3$. The collectivity of these $B(\mathrm{E3})$ values in ^{226}Ra is about three times larger than the one encountered in heavier actinide nuclei of octupole-vibration type.

4.2. COLLECTIVE DIPOLE MOMENTS

The electric dipole moments Q_1 are determined from the measured E1 matrix elements (table 2) and are shown in fig. 9 as a function of the angular momentum. One observes a marked increase with increasing angular momentum.

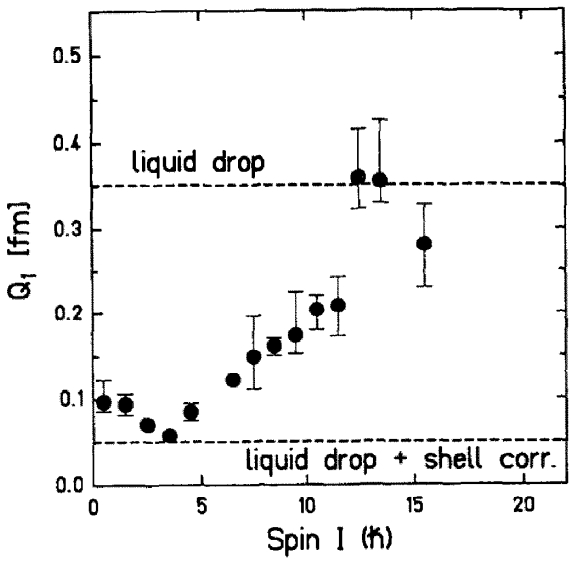

Fig. 9. Electric transition dipole moments, Q_1, for the yrast band in ^{226}Ra.

The large dipole moments may arise in the intrinsic frame due to a shift between the centre-of-charge and the centre-of-mass. As pointed out by Strutinsky [14]) and Bohr and Mottelson [15]) the dipole moment results from an interplay between the strongly attractive proton-neutron force represented by the symmetry-energy term and the Coulomb force. Using the two-fluid liquid-drop model it is estimated to be:

$$Q_1^{\mathrm{LD}} = C_{\mathrm{LD}} AZ(\beta_2\beta_3 + 1.458\beta_3\beta_4)\,, \tag{8}$$

where A and Z are the mass and charge number of the nucleus. For the Ra and light Th nuclei the $\beta_3\beta_4$ term is about as large as the $\beta_2\beta_3$ term and thus should not be neglected in eq. (8). For ^{226}Ra we assumed the deformation parameter β_4 to be constant and have the value determined from the hexadecapole moment measured at low spin. The quadrupole (β_2), octupole (β_3) and hexadecapole (β_4) deformation parameters for ^{226}Ra listed in table 1 were used to calculate the electric dipole moment Q_1 - using the liquid-drop formula (eq. (8)) with the constant $C_{\mathrm{LD}} = 5.2 \times 10^{-4}$ fm. The experimental data shown in fig. 9 seem to approach this theoretical value at high angular momenta, just as the energy levels in ^{226}Ra approach the stable-octupole limit above spin $I \sim 11\hbar$ (see fig. 6). The deviations of the experimental dipole moments Q_1 from the liquid-drop E1 moment of the observed shape (β_2, β_3, β_4) at low spins can only be explained by the influence of shell structure [16]), which almost cancels the liquid-drop contribution. Since the nuclear shape and especially the β_3 deformation remains constant (see fig. 8), the shell correction has to decrease with increasing angular momentum in order to explain the behaviour of the intrinsic dipole moments.

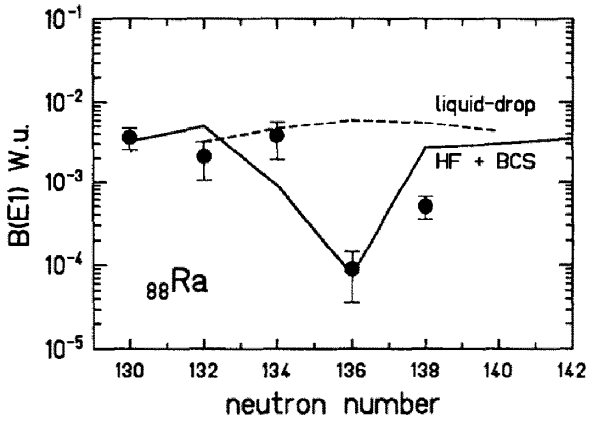

Fig. 10. Experimental and theoretical $B(E1)$ values for Ra isotopes at low spins ($I \simeq 5$).

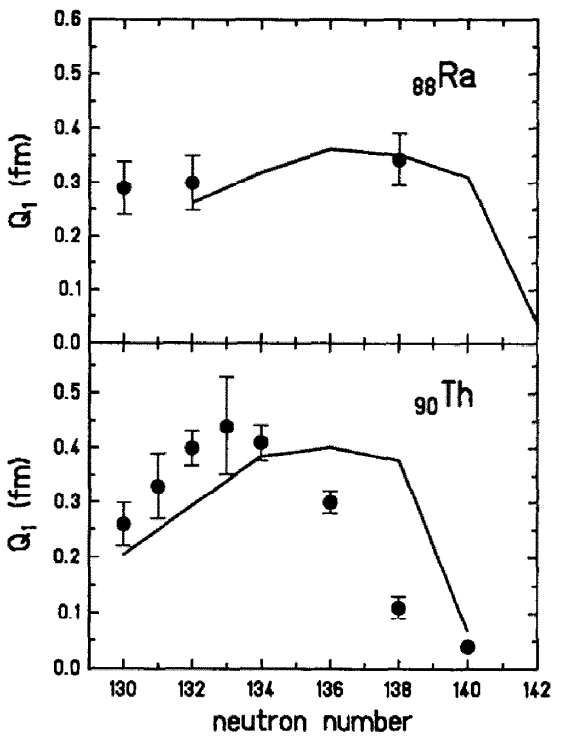

Fig. 11. Comparison of the experimental and liquid-drop dipole moments, Q_1, measured at medium high spins for Ra (top) and Th isotopes (bottom).

The influence of shell structure is also seen in neighbouring nuclei. Fig. 10 shows the $B(E1)$ values in Weisskopf units (W.u.) for the Ra isotopes, extracted for low spin states ($I \sim 5$) from the measured branching ratios [17-20]). In the framework of the liquid-drop model (eq. (8)) one expects that the absolute value of the E1 moment will grow with octupole deformation β_3. However, one observes the smallest E1 moment for ^{224}Ra for which the 1^- state is the lowest non-rotational state in all even-A nuclei. The intrinsic dipole moments in the Ra–Th region were recently calculated by Egido and Robledo [21]) using the HF+BCS model with the Gogny interaction. They obtained excellent agreement with experimental $B(E1)$ transition rates and, in particular were able to reproduce the very low values of Q_1 in ^{224}Ra. These calculations predict a decrease of the positive dipole moments to negative values in going from light Ra isotopes to the heavier ones, with a zero-crossing close to $A = 224$. This dependence has probably to do with gradual filling of the $j_{15/2}$ neutron shell. As a consequence, the measurement of E1 transition moments alone does not allow a unique determination of the octupole mass deformation.

Fig. 11 shows the systematics of the intrinsic electric dipole moments for Ra and Th isotopes at higher spin states ($I \sim 10$). The experimental data[17-20,22-24]) are compared to predictions of the liquid-drop model (eq. (8)) using the same constant C_{LD} as the one given above. The deformation parameters $\beta_2, \beta_3, \beta_4$ were taken from a calculation of Leander *et al.* [10]). One finds good agreement between the experimental dipole moments and the liquid-drop values, indicating that shell corrections are less important at higher spins. This result is consistent with the observed spin dependence of the measured dipole moments Q_1 in ^{226}Ra (see fig. 9).

The field of octupole deformed nuclei has dramatically expanded during the last years. In addition to the relatively well-explored Ra–Th region, there are further promising candidates for such collective modes: For the Ba–Sm ($Z \sim 56$, $N \sim 88$) nuclei [25-27]) low-lying negative-parity states, parity doublets, alternating-parity bands with enhanced E1 transitions have been established experimentally. In many cases the data are consistent with the assumption of a static nuclear octupole deformation. This deformation seems to stabilize with increasing rotational frequency, a feature which is not yet explained in a satisfactory way within the octupole model.

5. Summary

The spin-dependence of the collective properties of ^{226}Ra - transition energies and electric multipole moments - determined by Coulomb excitation is the main contribution of the present paper. The technique allows the measurement of E3 transition moments providing us with rich structural information about the physics of octupole instability. The E3 matrix elements can be related to the octupole deformation parameter β_3, and they are less sensitive to single-particle corrections than the E1 matrix elements. In the case of ^{226}Ra, the influence of the shell corrections on the E1 matrix elements seems to vanish at medium high spins so that the deduced

intrinsic electric dipole moments must be explained in a collective model. There are many experimental and theoretical indications that the octupole degree of freedom plays a key role in the structure of light actinide nuclei.

The authors thank the operating staff of the Tandem accelerator in Munich and the UNILAC in Darmstadt for providing excellent beam conditions. They are grateful to Dr. H.J. Maier for preparing the very delicate targets. They are also indebted to Prof. W. Nazarewicz for many valuable discussions. This work was partially supported by the Bundesministerium für Forschung und Technologie of the Federal Republic of Germany (#06 LM 171 I1) and by the Deutsche Forschungsgemeinschaft (Grant Bo 1109/1-1). P.A.B. acknowledges support from the U.K. Science and Engineering Research Council.

References

1) F.S. Stephens, F. Asaro and I. Perlman, Phys. Lett. **96** (1954) 1568; Phys. Lett. **100** (1955) 1543
2) R.K. Sheline, Phys. Rev. **C21** (1980) 1660
3) R.H. Spear, At. Data Nucl. Data Tables **42** (1989) 55
4) W. Nazarewicz and P. Olanders, Nucl. Phys. **A441** (1985) 420
5) J. Dudek, W. Nazarewicz and Z. Szymanski, Phys. Rev. **C26** (1982) 1708
6) R.S. Simon and F. Folkmann, Z. Phys. **A298** (1980) 121
7) R. Bengtson and S. Frauendorf, Nucl. Phys. **A327** (1979) 139
8) A. Winther and J. de Boer, in Coulomb excitation, ed. K. Alder and A. Winther (Academic Press, New York, 1966)
9) A. Lell, Diploma thesis, University Munich (1978), unpublished
10) G.A. Leander, R.K. Sheline, P. Möller, P. Olanders, I. Ragnarsson and A.J. Sierk, Nucl. Phys. **A388** (1982) 452
11) T. Czosnyka, D. Cline and C.Y. Wu, UR/NSRL Report 308/1987, University Rochester, unpublished
12) C. Fahlander, A. Bäcklin, L. Hasselgren, A. Kavka, V. Mittal, L.E. Svensson, B. Varnestig, D. Cline, B. Kotlinski, H. Grein, E. Grosse, R. Kulessa, C. Michel, W. Spreng and H.J. Wollersheim, Nucl. Phys. **A485** (1988) 327
13) A.S. Davydov and G.F. Filippov, Nucl. Phys. **8** (1958) 237
14) V.M. Strutinsky, Atomnaya Energiya **1** (1956) 150; J. Nucl. Energy **4** (1957) 523
15) A. Bohr and B.R. Mottelson, Nucl. Phys. **9** (1959) 687
16) G.A. Leander, W. Nazarewicz, G.F. Bertsch and J. Dudek, Nucl. Phys. **A453** (1986) 58
17) M. Gai, J.F. Ennis, D.A. Bromley, H. Emling, F. Azgui, E. Grosse, H.J. Wollersheim, C. Mittag and F. Riess, Phys. Lett. **B215** (1988) 242
18) P.D. Cottle, J.F. Shriner, F. Dellagiacoma, J.F. Ennis, M. Gai, D.A. Bromley, J.W. Olness, E.K. Warburton, L. Hildingsson, M.A. Quader and D.B. Fossan, Phys. Rev. **C30** (1984) 1768
19) W. Kurcewicz, N. Kaffrell, N. Trautmann, A. Plochocki, J. Zylicz, M. Matul and K. Stryczniewicz, Nucl. Phys. **A289** (1977) 1
20) E. Ruchowska, J. Zylicz, C.F. Liang, P. Paris and Ch. Briancon, J. Phys, **G18** (1992) 131
21) J.L. Egido and L.M. Robledo, Nucl. Phys. **A494** (1989) 85
22) W. Bonin, H. Backe, M. Dahlinger, S. Glienke, D. Habs, E. Hanelt, E. Kankeleit and B. Schwartz, Z. Phys. **A322** (1985) 59
23) P. Schüler, Ch. Lauterbach, Y.K. Agarwal, J. de Boer, K.P. Blume, P.A. Butler, K. Euler, Ch. Fleischmann, C. Günther, E. Hauber, H.J. Maier, M. Marten-Tölle, Ch. Schandera, R.S. Simon, R. Tölle and P. Zeyen, Phys. Lett. **B174** (1986) 241

24) M. Dahlinger, E. Kankeleit, D. Habs, D. Schwalm, B. Schwartz, R.S. Simon and P.A. Butler, Nucl. Phys. **A484** (1988) 337
25) W.R. Phillips, R.V.F. Janssens, I. Ahmad, H. Emling, R. Holzmann, T.L. Khoo and M.W. Drigert, Phys. Lett. **B212** (1988) 402
26) W. Urban, R.M. Lieder, W. Gast, G. Hebbinghaus, A. Krämer-Flecken, T. Morek, T. Rzaca-Urban, W. Nazarewicz and L.S. Tabor, Phys. Lett. **B200** (1988) 424
27) P.A. Butler, in Heavy ions in nuclear and atomic physics, ed. Z. Wilhelmi and G. Szeflinska (Adam Hilger, Bristol and Philadelphia, 1989), p. 295
28) R. Zimmermann, thesis 1980, unpublished
29) A.S. Davydov and A.A. Chaban, Nucl. Phys. **20** (1960) 499